Normal and Lateral Forces between Lipid Covered Solids in Solution: Correlation with Layer Packing and Structure

L. M. Grant† and F. Tiberg†*

*Physical and Theoretical Chemistry Laboratory, Oxford OX9 3QZ, United Kingdom, and †Institute for Surface Chemistry, SE-114 86 Stockholm, Sweden

ABSTRACT We report on the normal and lateral forces between controlled-density mono- and bilayers of phospholipid co-adsorbed onto hydrophobic and hydrophilic solid supports, respectively. Interactions between 1,2-dioleoyl-*sn*-glycero-3-phosphocholine layers were measured using an atomic force microscope. Notable features of the normal force curves (barrier heights and widths) were found to correlate with the thickness and density of the supported lipid layers. The friction and normal force curves were also found interrelated. Thus, very low friction values were measured as long as the supported layer(s) resisted the normal pressure of the tip. However, as the applied load exceeded the critical value needed for puncturing the layers, the friction jumped to values close to those recorded between bare surfaces. The lipid layers were self-healing between measurements, but a significant hysteresis was observed in the force curves measured on approach and retraction, respectively. The study shows the potential of using atomic force microscopy for lipid layer characterization both with respect to structure and interactions. It further shows the strong lubricating effect of adsorbed lipid layers and how this varies with surface density of lipids. The findings may have important implications for the issue of joint lubrication.

INTRODUCTION

Self-assembled phospholipid structures are abundant in all organisms and play vital roles in many biological processes. Cell plasma membranes consist of a mixture of phospholipids, glycolipids, and proteins and have an active role in cellular processes such as recognition, cell adhesion, and fusion (Voet and Voet, 1990). Lipid surface linings have also a key role of preventing contact formation, thus sustaining the membrane integrity by virtue of repulsive interactions between hydrated headgroups. Lipid layers appear furthermore to play a key role in joint lubrication and appear in the synovial fluid (Hills 1989, 1995; Johnston 1997; Schwarz and Hills, 1998). Other physiological lubricating sites where lipids are claimed to have a beneficiary lubricating function include pleura, pericardium, the ocular surface, and the gut where sliding occurs during gastric motility (Hills, 2000). Lipids are also important constituents in foods where they, besides their role as a basic nutrition also have functions as gelating agents, emulsifiers, and lubricants (Larsson, 1994). Most common food processes involve the transformation of organized biological tissues into the actual food product, which is further processed in vivo. It is clear that forces between and within lipid assemblies are important also in these processing stages.

A systematic force measurement study of interactions between lipid assemblies requires a flexible methodology for generating supported layers with tunable structural characteristics. Supported membranes have frequently been used as model systems for the purpose of studying interactions between surface-immobilized lipid assemblies. Besides their attractiveness as models for biological membranes, they have been proven highly useful for biofunctionalization of surfaces used for instance in the design of biosensors (cf. McConnell et al., 1986; Sackman, 1996). Langmuir-Blodgett (LB) deposition (Kop et al., 1984; Solletti et al., 1996), spin-coating (Malmsten, 1995), and adsorption and subsequent collapse of phospholipid liposomes (Bayerl and Bloom, 1990; Giesen et al., 1991; Johnson et al., 1991) are the most common approaches used for depositing supported layers. These methods are usually well designed but suffer from various drawbacks. LB deposition and spin-coating methods are for instance limited to flat surfaces and are also technically difficult. Adsorption from liposomal solutions involves kinetic limitations, which may lead to a poor reproducibility of the layer characteristics. In the current study, we have used a sequential adsorption and rinsing strategy for generating mono- and bilayer structures of lipids with controlled densities on hydrophobized silica and bare silica substrates, respectively. 1,2-Dioleoyl-*sn*-glycero-3-phosphocholine (DOPC) was co-adsorbed with *n*-dodecyl-β-maltoside (DDM) surfactant from aqueous solutions of different concentrations. The fraction of highly water-soluble DDM in these surface layers was selectively desorbed by rinsing with water. Subsequent adsorption from a less concentrated solution of DOPC and DDM increases the fraction of DOPC in the layer. This approach facilitates the build-up of layers with controlled lipid densities. The surface excess and thickness of the layers can during a deposition process conveniently be monitored in situ by, e.g., the use of null ellipsometry (Tiberg et al. 2000).

Quite a number of studies of force interactions between lipid layers have been executed and published over the years, at first by using the osmotic stress technique (Lis et

Submitted March 26, 2001, and accepted for publication December 14, 2001.

Address reprint requests to Fredrik Tiberg, Institute for Surface Chemistry, P.O. Box 5607, SE-114 86 Stockholm, Sweden.

0006-3495/02/03/1373/13 $2.00

al., 1982) and the surface force apparatus (SFA) (Afshar-Rad et al., 1986; Israelachvili, 1994; Marra, 1985; Marra and Israelachvili, 1985). These studies have provided quite a detailed account for the long-range van der Waals and electrostatic forces and short-range steric/hydration interactions between membranes. Direct force measurements by use of the SFA are, however, generally limited to mica substrates and to the use of relatively low contact pressures. Atomic force microscopy has in later years emerged as a versatile tool for measuring forces between supported surfactant and lipid layers and for imaging of in-plane layer structures (cf. recent reviews by Manne and Gaub, 1997; Senden, 2001; Tiberg et al., 1999; Warr, 2000). Benefits of the AFM for force measurements include (Capella and Dietler, 1999) the ability to perform lateral and normal force measurements in gas and liquid media with contact areas in the molecular-to-colloidal size range, small sample volume, versatile choice of substrates, and the possibility to follow dynamic interfacial structuring phenomena and effects of controlled perturbations. Furthermore, the high spatial resolution obtained using sharp tips enables imaging of surface structure in the plane of the surface and correlating forces and topography. Drawbacks of AFM compared with more macroscopic force probes include a lower sensitivity in terms of force per unit area, an uncertainty of probe geometry in the contact region, and no independent means of determining the surface separation. A large number of normal force and imaging studies have during the years been carried out on adsorbed/supported surfactant and lipid layers. Published work on normal forces between lipid layers chiefly concern LB deposited layers (Dufrene and Lee, 2000). Dufrêne and co-workers (Dufrene et al., 1997, 1998; Schneider et al., 2000) have measured normal force curves on mica and fitted these data using a combination of steric/hydration interactions and contact mechanics. These studies, as many others on surfactant and lipid systems, highlighted the importance of mechanical interactions and the fact that the layers generally are ruptured at some critical applied load. A detailed description of the short-range interactions is, however, still missing, and deconvoluting and quantifying the contribution from different forces is clearly nontrivial (Capella and Dietler, 1999). Ducker and colleagues (Ducker and Clarke, 1994; Ducker et al., 1997) measured normal and lateral forces between adsorbed short-chain phospholipid layers at silicon nitride surfaces. The lipid layers were found to be strongly lubricating, but no obvious relation to the normal force curve characteristics was noted.

The present work involves a detailed examination of the relation between normal and lateral force interactions between supported lipid layers, interpreted in the light of interfacial structural properties. Force-distance and friction-load curves were measured between an AFM silica tip and flat hydrophobized silica and hydrophilic untreated silica surface, respectively. The measurements were performed in the absence and presence of supported mono- and bilayers of DOPC formed at the different surfaces by the earlier described co-adsorption and rinsing scheme. In addition, the in- and out-of-plane characteristics of the supported layers were characterized in situ by contact-mode AFM imaging and by null ellipsometry. It is found that friction and normal force curves are interrelated and furthermore depend strongly on the lipid density in the adsorbed films but not significantly on the presence of co-adsorbed dodecyl maltoside surfactant. The results also suggest that adsorbed DOPC layers can resist substantial normal loads and provide efficient boundary lubricants in such situations. This finding appear to have important implications for the issue of joint lubrication as well as for quantitative modeling of friction force data obtained between macroscopic surfaces.

MATERIALS AND METHODS

Materials

DOPC was purchased from Fluka Chemicals. The purity of the reagent was ≥99% with respect to both its dioleoyl chain length and the headgroup composition. DOPC was solubilized using DDM (Sigma Chemical Co., St. Louis, MO; purity > 98%, molecular weight = 510.6 g/mol). The critical micellar concentration of the surfactant has been reported as 1.67×10^{-4} mol/L (0.085 g/L) (Hines et al., 1998). Both substances were used without further purification. Water was purified by distillation followed by deionization in an ion-exchange unit and then passage through a Milli-Q RG system consisting of charcoal filters, ion-exchange media, and a 0.2-μm filter. Hydrophilic silica substrates were prepared from polished silicon test wafers (Okmetic) that had been oxidized thermally in a saturated oxygen atmosphere at 920°C for 1 h, followed by annealing and cooling in an argon flow. This procedure results in a SiO_2 layer with a thickness of ~30 nm. The wafers where then cut into slides of width ~12 mm. The hydrophilic silica slides were before use cleaned by heating at 80°C for 5 min in solutions of 1) a mixture of 25% ammonia (Pro Analysi, Merck), 30% H_2O_2 (Pro Analysi, Merck), and H_2O (1:1:5 by volume) and 2) a mixture of 32% HCl (Pro Analysi, Merck), 30% H_2O_2 (Pro Analysi, Merck), and H_2O (1:1:5 by volume). The slides were then rinsed twice, first in distilled water and then in ethanol, and were stored in ethanol until use. The advancing and receding water contact angles for these slides were $\theta_{adv} = 8°$ and $\theta_{rec} = <5°$. Before use these slides were cut into squares of suitable size for the AFM measurement cell, then rinsed thoroughly with Milli-Q water, and finally subject to plasma cleaning (Harrick Scientific) for 5–10 min. Hydrophobized silica substrates were prepared by exposing clean hydrophilic slides to dimethyloctylchlorosilane vapor in a vacuum chamber for 24 h. These hydrophobized slides were then washed in trichloroethylene, hexane, and ethanol to remove excess dimethyloctylchlorosilane. The contact angles for these slides were $\theta_{adv} = 105°$ and $\theta_{rec} = 96°$.

Ellipsometry

The substrates used for the ellipsometric measurements were oxidized silicon wafers. Before performing the adsorption measurements these surfaces were pretreated as described above. The instrument used for characterizing the co-adsorption process and structure formation on the bare oxidized silica substrates was a modified Rudolph Research thin-film ellipsometer, type 43603–200E, equipped with high-precision stepper motors. The machine has an angle resolution of 1/1000°. The experimental setup and the measurement procedures are described in detail in the

original reference (Tiberg et al., 2000). Here we present only selected results as a background and reference to the interaction force measurements made by use of AFM. The ellipsometric technique allows simultaneous measurements of the mean thickness and refractive index (or density) with a good time resolution, ~2 s. The thickness resolution during in situ measurements of lipid or surfactant films adsorbed at silica from aqueous surfactant solution was typically ±3 Å (Tiberg, 1996).

Atomic force microscopy

In this paper all data were obtained with a Nanoscope III AFM using a single, 348-μm-long, rectangular cantilever (Silicon MDT), and the spring calibrations were performed after the measurement. All measurements were performed using the same silica tip. The radius of the tip was ~70 nm as determined from a scanning electron microscopy image. Using the same cantilever in each experiment allows comparisons between different force measurements, assuming that the cantilever characteristics remain unchanged. The rectangular geometry was chosen as these cantilevers exhibit a near linear relationship between lateral force and torsion angle. The normal spring constant of 0.23 ± 0.02 Nm^{-1} was determined by measuring the change resonant frequency of the loaded and unloaded cantilever. The lateral spring constant was calculated from the dimensions of the cantilever, which gave a value of 2.3 ± 0.4 nNm rad^{-1}. The calibration constant relating the lateral voltage signal to the tilt angle of the probe was determined by using a mirror instead of a cantilever for reflection of the laser into the detector. The lateral detector voltage was recorded as the mirror was tilted a known angle with a stepping motor. This procedure provides the lateral sensitivity of the photodiode.

The images shown are deflection images with low integral gains and a scan rate of 10 Hz. The force curves shown in this study were mostly obtained at a scan rate of 1 Hz, corresponding to a lateral tip movement speed of 0.5 μm/s. Variation between 0.2 and 20 Hz resulted in no significant changes in the output results. For the friction measurements high integral gains of up to three were used to ensure that the normal force exerted on the adsorbed layer remained constant throughout the measurement of each friction loop. For the data presented here the lateral range of movement of the scanner during the friction measurements was 200 nm and the scan rate was 2–40 Hz, corresponding to rates of 0.4–8 μm/s.

RESULTS AND DISCUSSION

Adsorbed layer properties on silica, images and comparison with ellipsometry data

Stable and reproducible DOPC surface layers were produced at silica and hydrophobized silica surfaces by coadsorbing DOPC and DDM at the silica surface from mixed micellar solutions according Tiberg et al. (2000). (The DOPC-DDM concentrations in this original work were erroneously given to be three orders of magnitude lower than the correct values presented in this study.)

The adsorption and rinsing procedure used to prepare supported lipid layers for the AFM measurements may be outlined as follows: initial adsorption from a 0.114 g/L DOPC-DDM solution (stage 1), rinsing of 2 ml of water every 5 min for 50 min (stage 2), readsorption from a 10 times diluted 0.114 g/L DOPC-DDM solution (stage 3), a further water rinsing step identical to stage 2 (stage 4), a second readsorption step from a $2.85\ 10^{-3}$ g/L DOPC-DDM solution (stage 5), and a final rinsing step identical to stages 2 and 4 (stage 6). For convenience, the above steps will be referred to as stages 1–6 throughout the rest of this work. All concentrations refer to the total concentration of DOPC and DDM at a constant 1:6 ratio of DOPC to DDM.

Figs. 1, *A–C*, shows ellipsometry data measured for adsorbed layers at stages analogous to those described above. Due to differences in the experimental setup between the two instruments the procedures could not be made identical. The only differences between the method described above and the deposition procedure used in Tiberg et al. (2000) are a 1) continuous rinsing of water during stages 2, 4, and 6 (~20 ml/min) and 2) additional rinsing and readsorption steps in between stages 2 and 3 and 5 and 6. These additional stages are not shown in Fig. 1 but are described in the original publication (Tiberg et al., 2000) and are displayed here only for comparison. A brief outline of the ellipsometry results is given in the following paragraph.

A relatively rapid linear increase of the surface excess with time was observed after the first addition of 0.14 g/L DOPC/DDM, see Fig. 1 *A*. A plateau adsorption value of 4.1 mg/m^2 was in this first adsorption cycle reached within ~250 s. A plateau layer thickness of 4.4 nm is established much earlier, and further adsorption results only in a densification of these surface layers. When rinsing with water (20 ml/min) is started after 1500 s, we note that the surface excess first decreases rapidly and then a new plateau adsorption value is established around 2.8 mg/m^2; i.e., rinsing results in desorption of about 24% of the originally adsorbed amount. However, when rinsing after readsorption from a less concentrated solutions is done, a very limited desorption is noted, see Fig. 1, *B* and *C*. The calculated surface excess of DOPC on silica was after the final rinsing step 4.2 mg m^{-2}, giving an average headgroup area per DOPC molecule of 0.62 nm^2. For the same headgroup area in the lamellar phase, Lis and co-workers (1982) and Bergenståhl and Stenius (1987) measured a bilayer thickness of about 4 nm. This agrees well with the bilayer thickness shown in Fig. 1, *A–C*. Considering the fact that molecular solubility of DDM is orders of magnitude higher than lecithin and that desorption rate is proportional to solubility (Brinck et al., 1998; Tiberg et al., 1994), it is possible to infer that the adsorbate remaining at the surface after the last rinsing step is complete consists almost exclusively of DOPC. Note that DDM has no affinity for the silica surface by itself. No adsorption at silica from pure DDM solutions could be detected using ellipsometry (Tiberg et al., 2000). The above indicates that we are able to deposit DOPC layers with a controlled lipid density at solid substrates by sequential adsorption and rinsing procedures and by choosing the appropriate solution concentration of the DOPC-DDM system during the adsorption stage.

The density of surface-bound DOPC is in response to rinsing stages from more concentrated solutions reduced (see stages 2 and 4 in Fig. 1, *A* and *B*). AFM images obtained below the critical breakthrough force (see below) were for all adsorption stages featureless as is shown in Fig.

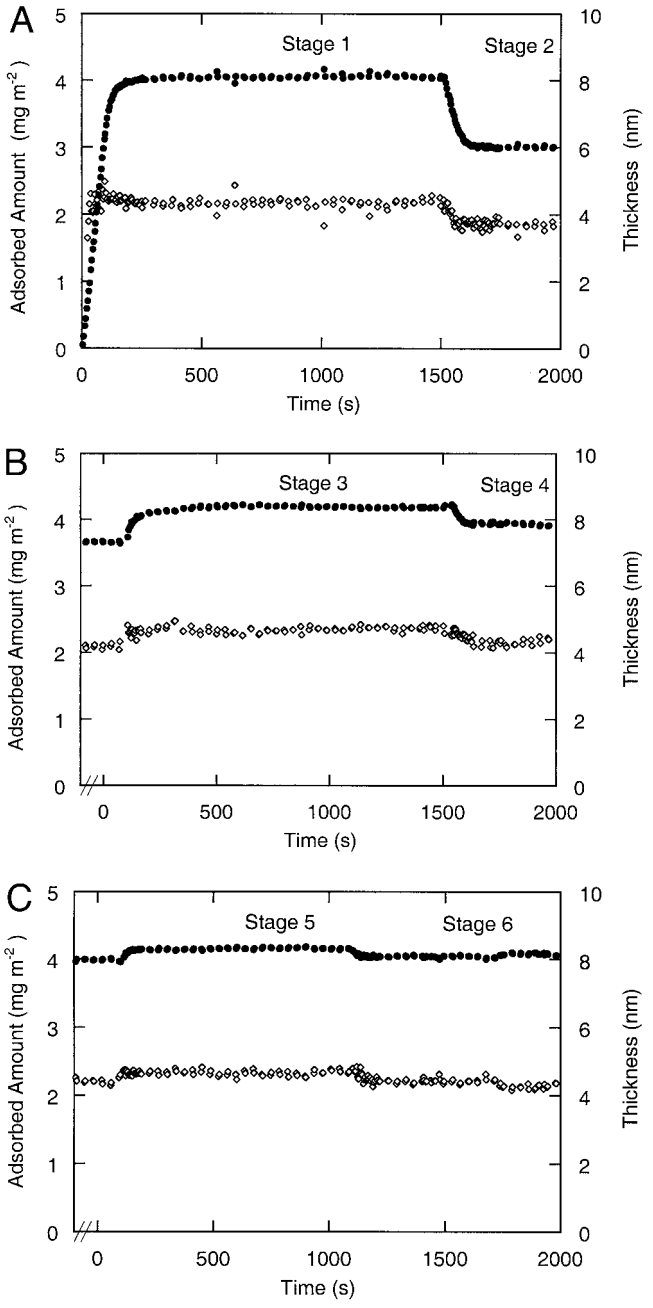

FIGURE 1 (*A*) Time evolution of the adsorbed layer thickness (◇) and the surface excess (●) during adsorption onto bare silica from a 0.114 g/L micellar solution of DOPC and DDM (stage 1) and, after 1500 s of rinsing, was performed with a continuous flow of DD-MP water (stage 2); (*B* and *C*) Corresponding evolution during readsorption experiments from less concentrated DOPC-DDM solutions (1:6 by weight) of concentrations 1.14 10^{-2} g/L and 2.85 10^{-3} g/L (stages 3–4). All curves are redrawn from Tiberg et al. (2000). Plateau conditions at stages 1–6 indicate the conditions at which the force curves have been measured in this work. Note that additional adsorption and rinsing steps were performed between stages 2–3 and 4–5 in the adsorption study, in which the concentrations are erroneously are claimed to be three orders of magnitude lower than indicated above.

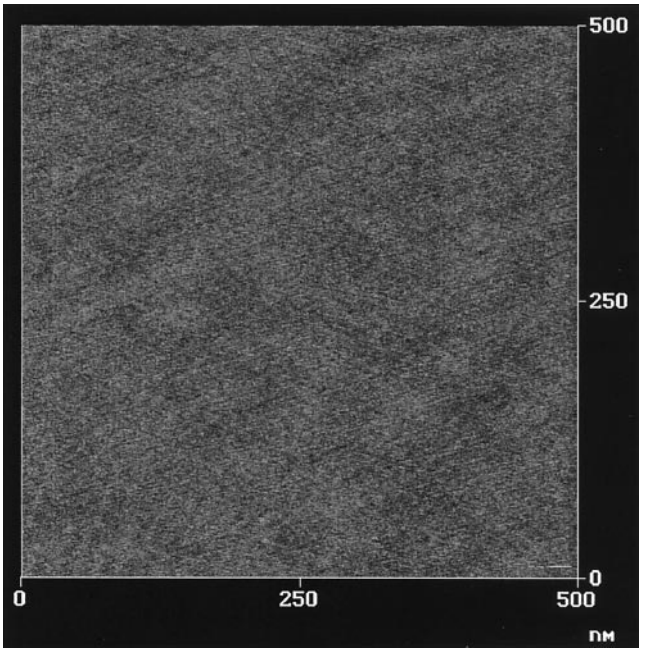

FIGURE 2 An atomic force microscopy image of the adsorbed layer at stage 2 on hydrophilic silica. Other solution conditions produced very similar images. No changes in the appearance of the image were observed with increasing force until the mechanical instability of the film was reached and surface features were imaged. From the laterally homogenous character of these images together with the thickness of the layer from the force curves (Fig. 3) and ellipsometry data (Fig. 1) it is inferred that a continuous bilayer structure is formed on this surface. Similar featureless images were obtained at all stages (1–6) studied, i.e., at all surface coverages of DOPC and DDM.

2, thus indicating that the surface layer is not built of discrete aggregates but always is more or less continuous DOPC films that have different lipid packing densities. It is important to note that if defects exist on a scale of less than 2–3 nm they would not be easily detected in contact imaging mode.

Normal forces between adsorbed bilayers on silica

Normal force versus distance curves measured during approach and separation cycles on silica surfaces covered by DOPC/DDM layers are shown in Fig. 3. The graphs correspond to different stages in the adsorption-rinsing stages shown in Fig. 1. These curves display a number of common features. Upon examining the approach curves, we note that there is no observable long-range electrostatic force contribution. The onset of repulsive force occurs at 7–8 nm. As the separation distance is decreased the repulsive force rises proportional to the decrease in separation until the maximum mechanical stability of the film is reached at a distance of roughly 4 nm. At shorter separations, the surfaces jump into hard-wall contact.

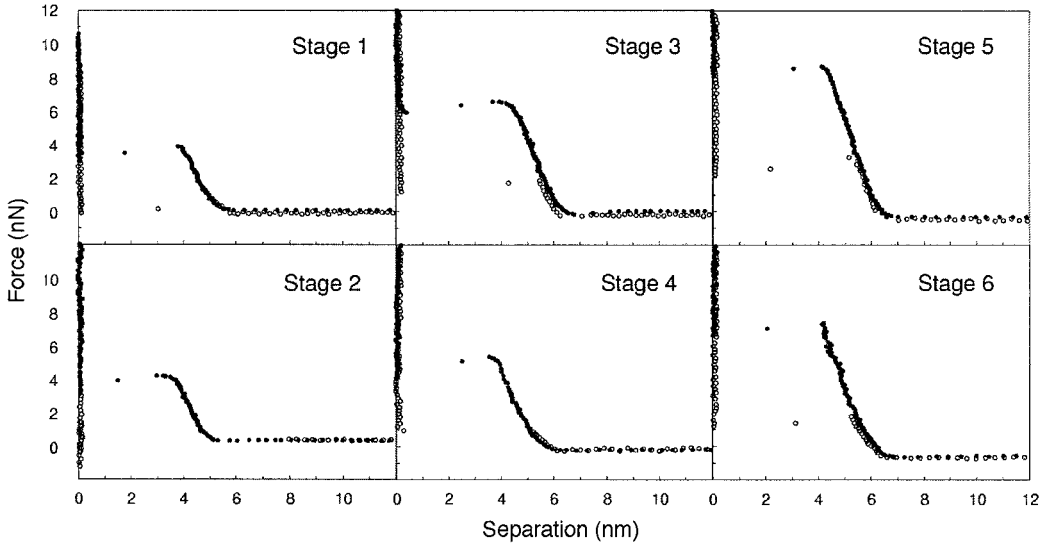

FIGURE 3 The normal force-versus-distance profiles for the mixed DOPC and DDM layers adsorbed at the silica solution interface measured ~20 min after the readsorption and the rinsing stages 1–6 (●, approach; ○, retraction). Notably, substantial increases in the height of the steric barrier occur when more DOPC is adsorbed (stages 3 and 5) even though the increase in the total amount of material is negligible between stages 1, 3, and 5 (see Fig. 1). Also, each time water was rinsed through the cell only small decreases in both the height of the barrier and the distance where an interaction was measurable occur, indicating that the layer thickness and stability of the layer decreases slightly. There is no adhesion on retraction except for stage 2 where a small adhesion of ~1 nN is observed. The barrier height of the retraction curve increases through the stage sequences 1, 3, 5 and 2, 4, 6, suggesting that surface pressure of the film is large enough to reform the adsorbed layer at low loads.

When the tip is retracted away from the flat substrate, the surfaces adhere until the applied load is reduced below a critical pull-off value after which the surfaces jump out of contact. Beyond this point, the force curves measured on approach and separation are virtually superimposed.

The repulsive force onset distance of 7–8 nm agrees well with the thickness of two DOPC bilayers, and the jump at a distance of slightly more than 4 nm is similar to the ellipsometric thickness of one bilayer (4.4 nm). This value also compares well with the bilayer thickness of about 4.3 nm in the concentrated lamellar phase measured by Lis et al. (1982) and Bergenståhl and Stenius (1987). The jump-in apparently corresponds to penetration of the inner bilayer bound to the flat silica substrate, probably with the majority of the low-solubility DOPC moving out of the contact area. We suggest that a bilayer structure is present also at the tip and that this layer is removed at lower loads than the material bound to the underlying silica surface. Support of this notion includes the fact that the surface chemistry of the tip and underlying substrate in both cases is silica and that the force onset separation is comparable to the thickness of two bilayers. The supposition is furthermore in keeping with the observation that a much steeper force barrier is observed when pushing together two macroscopic surfaces covered by surfactant bilayers (Tiberg and Ederth, 2000). The jump-in distance corresponded in this study to the expulsion of two bilayers.

In a recent study where the forces between surfaces covered by surfactant bilayers were studied by AFM using force probes of different sizes, we also noted a change in the jump-in distance from one to two bilayer thickness when increasing the size of the probe (work in progress). For intermediate sizes, the expulsion proceeds in two steps corresponding to expulsion of bilayers one after the other. In several AFM studies of forces between adsorbed layers by AFM, the region from repulsive force onset to jump-in is interpreted as a measure of hydration interactions and layer compression. The possibility of compressing and displacing adsorbate at the tip at lower forces is seldom acknowledged, although this process may strongly affect the shape of the force curve in this region. This may also be the case when studying, e.g., LB deposited supported layers, since material may easily be transferred from the substrate to the tip.

In Fig. 3 it can be seen that the barrier height measured on approach changes with both the adsorption density and composition of the surface-bound bilayers. The barrier height increases with a factor of roughly two when going from stage 1 to 5 in the presence of DDM as well as when going from stage 2 to 6 after rinsing and desorption of the more soluble DDM fraction. By comparing adsorption data and force curves, we see that the large DDM fraction adsorbed at stage 1 compared with stage 2 has only a minor influence on the measured forces. However, small increases of the surface density of DOPC have a major effect. This is likely to be related to the relative affinity of DOPC and

DDM for the solid surface and magnitude of the lateral interactions between the different lipophilic tails.

We suspect that the barrier height may be correlated to the surface pressure exerted by the adsorbed film, which will be strongly dependent on the surface density of DOPC at the solid surface. Unfortunately, we had no alternate means of measuring the surface pressure of the adsorbed film. We can, however, from the measured force $F(H)$ at distance H estimate the energy per unit area $E(H)$ that is necessary for displacing the adsorbed layer (Derjaguin, 1934):

$$E(H) = F(H)/2\pi R$$

The estimated energies obtained from breakthrough forces range between 8 mN/m for the force curve measured at stage 1 to about 20 mN/m for the densest adsorbed lipid bilayer obtained at stage 6. Similar numbers were obtained for the monolayer systems adsorbed at the hydrophobic surface discussed below.

The force curves measured on approach and separation reveal a hysteresis in the region where jump-in and jump-out are observed. The fact that the force curves are not reversible may be in part explained by energy dissipation occurring during the squeezing out of the bilayer from the contact zone or a kinetically limited healing process of the layer when the applied load is reduced. The layer relaxation is rather slow, as the curves were not significantly affected when the rate of approach and separation was varied between 0.4 μm/s and 4 μm/s. A similar slow relaxation was also observed in a previous surface force study of similar adsorbate layers (Tiberg and Ederth, 2000). Another possibility is that some material becomes irreversibly trapped in the contact zone leading to strong contact adhesion. It should be noted that virtually no contact adhesion was observed in the absence of adsorbed DOPC.

An interesting feature of the force curves measured during separation is the fact that the surfaces with higher DOPC content cause the tip to be pushed out at positive applied loads. This effect is quite possibly related to the surface pressure exerted by the films surrounding the contact zone, which acts to reform the surface layer as the normal load is reduced. The size of the hysteresis increases only marginally with the layer density.

The normal force curves in Fig. 3 show only a very minor adhesive force before the repulsive force barrier is encountered. Earlier studies by Marra and Israelachvili (1985) of forces between bilayers deposited at mica show clear adhesion minima. Similar adhesion minima were reported by Ducker and Clarke (1994) for the case of silicon nitride surfaces bearing bilayers of short-chain lipids. The absence of an adhesion minimum in the present study may be related to fact that the Hamaker constant of silica is lower. Compared with, for instance, silicon nitride, there is a difference of nearly one order of magnitude (cf. Capella and Dietler, 1999).

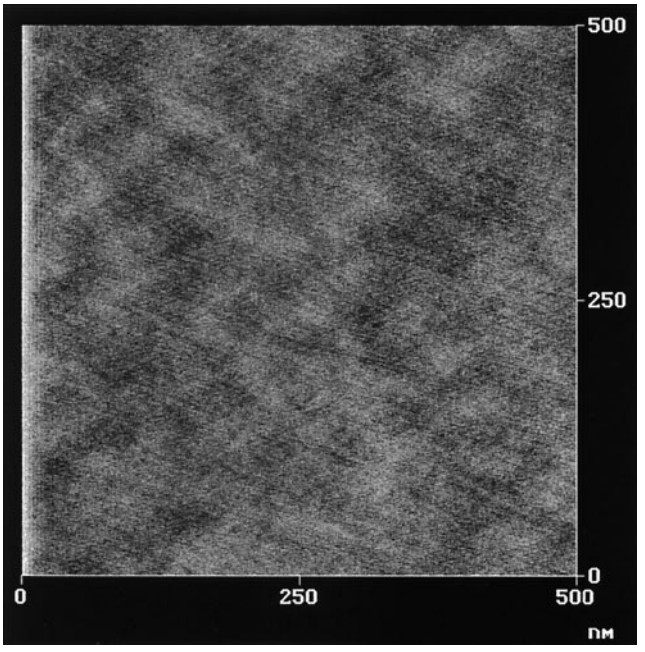

FIGURE 4 Atomic force microscopy image of the adsorbed layer at the hydrophobized silica surface measured at stage 2. Other solution conditions again produced very similar featureless images. For the images obtained on the hydrophobic substrate the underlying topography of the surface is reflected. However, no small-scale features that would suggest discrete aggregates or nonuniform layers were observed. From these images and the thickness of the layer from the force curves in Fig. 5, we infer that monolayer structure forms at this surface.

The jump-in at a separation corresponding to approximately one bilayer has been observed in a number of studies on interactions between surfactant-covered surfaces (Ducker and Grant, 1996; Grant and Ducker, 1997; Grant et al., 2000; Tiberg and Ederth, 2000) as well as between surfaces covered by shorter-chain lipids (Ducker et al., 1997; Schneider et al., 2000). In a study of force interactions between surfaces with adsorbed block copolymers, the breakthrough force was quantitatively correlated to the calculated surface pressure exerted by the copolymer layers (Eskilsson et al., 1998).

Normal forces measured between surfaces in the asymmetric system with a lipid monolayer present on the underlying hydrophobized silica support

Normal force curves were also measured with hydrophobized silica surface as the underlying substrate. Adsorption on the hydrophobic surface from DOPC-DDM solutions is expected to result in the formation of a monolayer structure with the aliphatic chains oriented toward the surface and the polar headgroups toward the aqueous

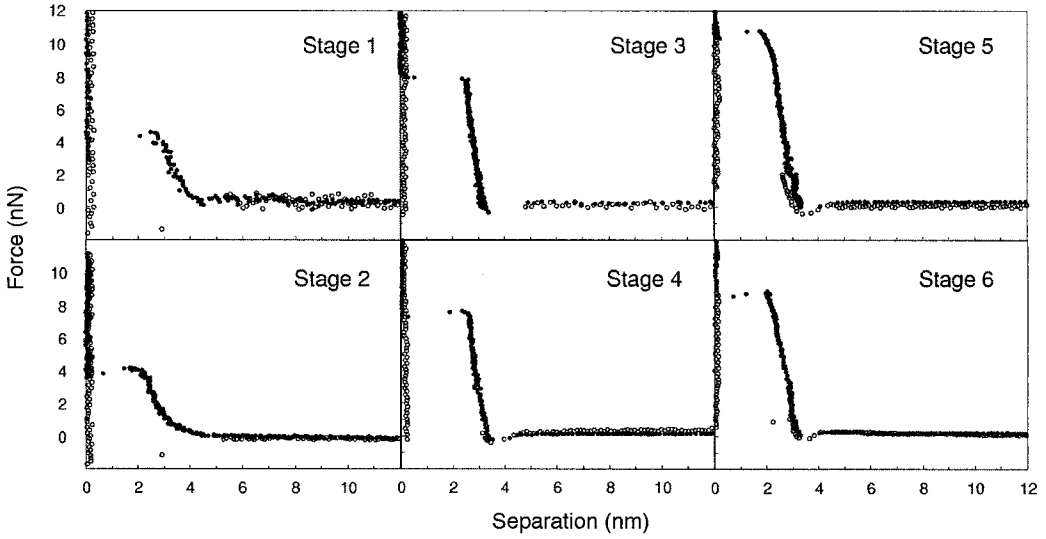

FIGURE 5 Force distance profiles between the AFM silica tip and hydrophobized surface, where both surfaces have been covered with mixed layers of DOPC and DDM. These curves are qualitatively similar to those in Fig. 3 but also reveal important differences, including the following: (*A*) the force-onset is seen at a smaller separation; (*B*) the slope of the barrier is steeper, indicating adsorption of a less compressible layer; (*C*) the critical force needed to puncture the layers is slightly larger for the later stages 3–6; and (*D*) an attraction minimum is also observed for stages 3–6 before the steric barrier is reached.

phase. Fig. 4 shows the surface topography of the DOPC-covered surface at stage 2. The large-scale features seen in the image are also seen on the bare hydrophobized wafer, although these features are slightly masked by the adsorbed layer. Once again no discernible surface features that would indicate the presence of domains or discrete surface aggregates were observed at this surface. In addition, the jump-in distances in Fig. 5 indicate the thickness on only one lipid layer. From these pieces of information we infer a monolayer film coverage at the hydrophobic surface at all examined DOPC/DDM ratios.

Fig. 5 shows the force versus distance curves measured after different adsorption-rinsing sequences. The main characteristics of these force curves are similar to those obtained using the bare silica surface as the base substrate. However, a number of distinct differences are observed. First, we see that the force onset is shifted to smaller surface-to-surface separations. Second, an attractive minimum is observed before the onset of the repulsive force barrier from stage 2 and on. The attractive minimum is followed by a steep repulsive barrier, again with a height that increases with increasing density of DOPC in the surface layer. The barrier heights observed for the asymmetric substrate system (Fig. 5) are only slightly larger than those measured for the symmetric system (Fig. 3), indicating that the lipid substrate interactions are less important than tail-tail interactions within the supported layer. The surface separation at which the surfaces jump into contact is for all force curves measured in the approach mode slightly larger than 2 nm, which is in good agreement with the assumption that adsorption from the DOPC-DDM solution results in the formation of a monolayer at hydrophobic surfaces. The maximal extension of one DOPC molecule from bond length and Van der Waals radii is about 2.5 nm. This also supports the earlier claim that the layer bound to the highly curved tip is removed at a lower force, before the surface-bound layer. As for Fig. 3, the force required to puncture the monolayer and establish surface-surface contact increases with increased lipid coverage density, but rinsing with water has again a much smaller effect. For both the symmetric silica-silica and asymmetric silica-hydrophobic silica systems, there is a noticeable effect after rinsing between stages 5 and 6. The fact that the observed barrier height decreases going from stage 5 to 6 is probably caused by a small change in the DOPC density rather than desorption of DDM, as the fraction of DDM in the surface layers at silica and hydrophobic silica should be very small.

A pronounced force minimum before the onset of the repulsive barrier is present in the force curves measured at stages 3–6 in Fig. 5. However, this is not visible in the force profiles obtained at stages 1 and 2. The adsorption at stage 1 is performed from a more concentrated solution, which results in a monolayer with a relatively large fraction of DDM. The absence of the adhesion at stage 1 could in this case be due to the hydration forces acting between strongly maltoside headgroups of the DDM surfactant. However, the absence of an adhesive minimum is also seen in the force-distance curve measured at stage 2, where most of the DDM is selectively desorbed during the rinsing process. The attractive minimum is observed

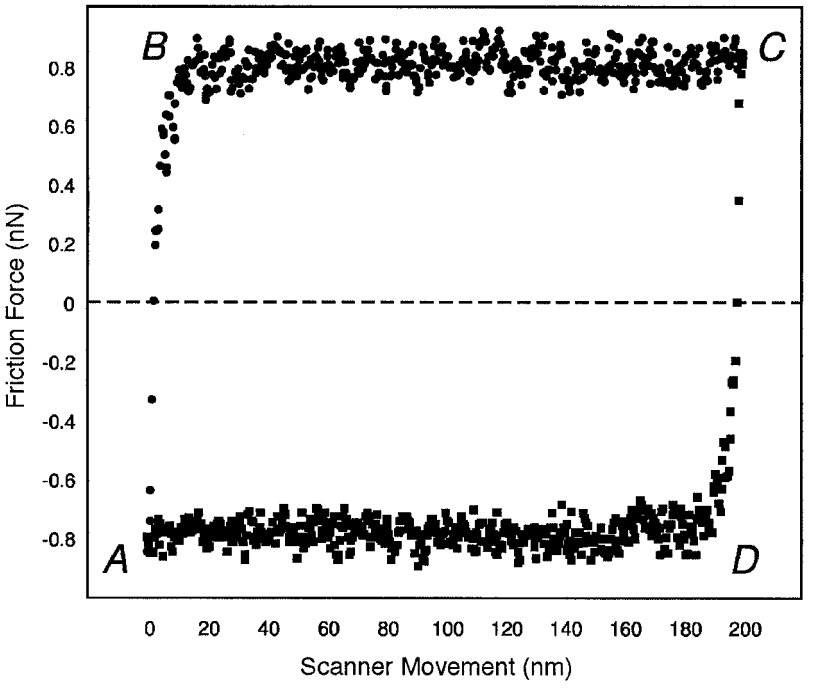

FIGURE 6 An example of a friction loop used to calculate the friction force of one point in Fig. 7. This loop is one cycle from a continuous rastering process so that the measured data are not usually from the first scan over the area. Initially the tip moves with the sample from point *A* to point *B*, held by adhesive interactions. At point *B* the cantilever exerts enough force to overcome the static friction force. Sliding between the tip and the sample then occurs. The regions *AB* and *CD* are, respectively, known as the static and dynamic regions of friction. When the direction of the scan is reversed at point *C* the tip again moves with the sample until sliding occurs at point *D*. The scan continues until the tip regains its original position. The twisting of the cantilever inverts when the scan direction is reversed; the region *ABC* is defined as positive lateral deflection and *CDA* negative. The friction is thus measured twice, to a large extent averaging out irregularities due to surface roughness or direction-dependent friction. The value of the friction force is taken as half the force difference between the two scans.

only when measuring the force between the tip and the monolayer structures denser in DOPC at the flat underlying support and not for the bilayer or less dense monolayer structures featured in Figs. 3 and 5 (stages 1 and 2). This suggests that the molecular organization is important for the steric/hydration interaction. The attraction could be due to Van der Waals forces; however, we are unable to explain the sudden appearance of this minimum in force.

Friction forces between bilayers adsorbed on silica

Friction force microscopy (FFM) involves the scanning of an AFM probe back and forth along a contact line while recording the cantilever torque through the horizontal deflection of the laser beam. An example of a friction measurement performed in water between an oxidized silicon tip in contact with an oxidized silicon wafer is shown in Fig. 6. The friction force is defined as the average of half the lateral force value between the lines BC and DA in Fig. 6, as the friction force is actually measured twice, once in each direction. The lateral spring constant and photodiode sensitivity are used to convert the raw data to qualitative values.

Fig. 7 shows the friction force versus load curves obtained using the symmetric silica tip-silica surface system at different adsorption stages. Each point represents an average of the dynamic friction values measured in a loop at constant applied load. All measurements were performed at relatively low loads between 0 and 12 nN. The solid line shows the friction force between bare silica in water. The loading and unloading portions of the applied load versus friction force curves showed no hysteresis when measured between bare surfaces in cycles of increasing and decreasing load. The calculated friction coefficient for the silica-silica system in water is ≈ 0.11. The friction force dependence on the normal load follows the phenomenological relation known as Amantons' law, which Bowden and Tabor (1967) attributed to the shearing of multiple asperity contacts that plastically deform by the applied load. The linear relationship between friction and normal force is ascribed to the linear increase of the total area of contact with increasing normal load. The friction between deforming bodies has been a subject of much discussion, and several models have been proposed for rationalizing the data. An in-depth discussion of this issue is, however, not within the scope of the present work. Instead we will focus on the effect that the DOPC layer density has on the friction.

The friction force measured between silica surfaces with the different density DOPC bilayers are shown in Fig. 7, *A* and *B*. The results obtained show a strong correlation with normal force curves in that the normal loads where the lipid layers are punctured or healed coincide with the loads where a sudden increase or decrease in friction force is observed; see Figs. 3, 7, and 8. Very similar sets of curves were obtained when measuring at stages 1, 3, and 5, i.e., in the presence of coadsorbed DDM, and stages 2, 4, and 6, where most DDM has been desorbed. The friction force was measured in cycles of increasing and decreasing loads. Starting with

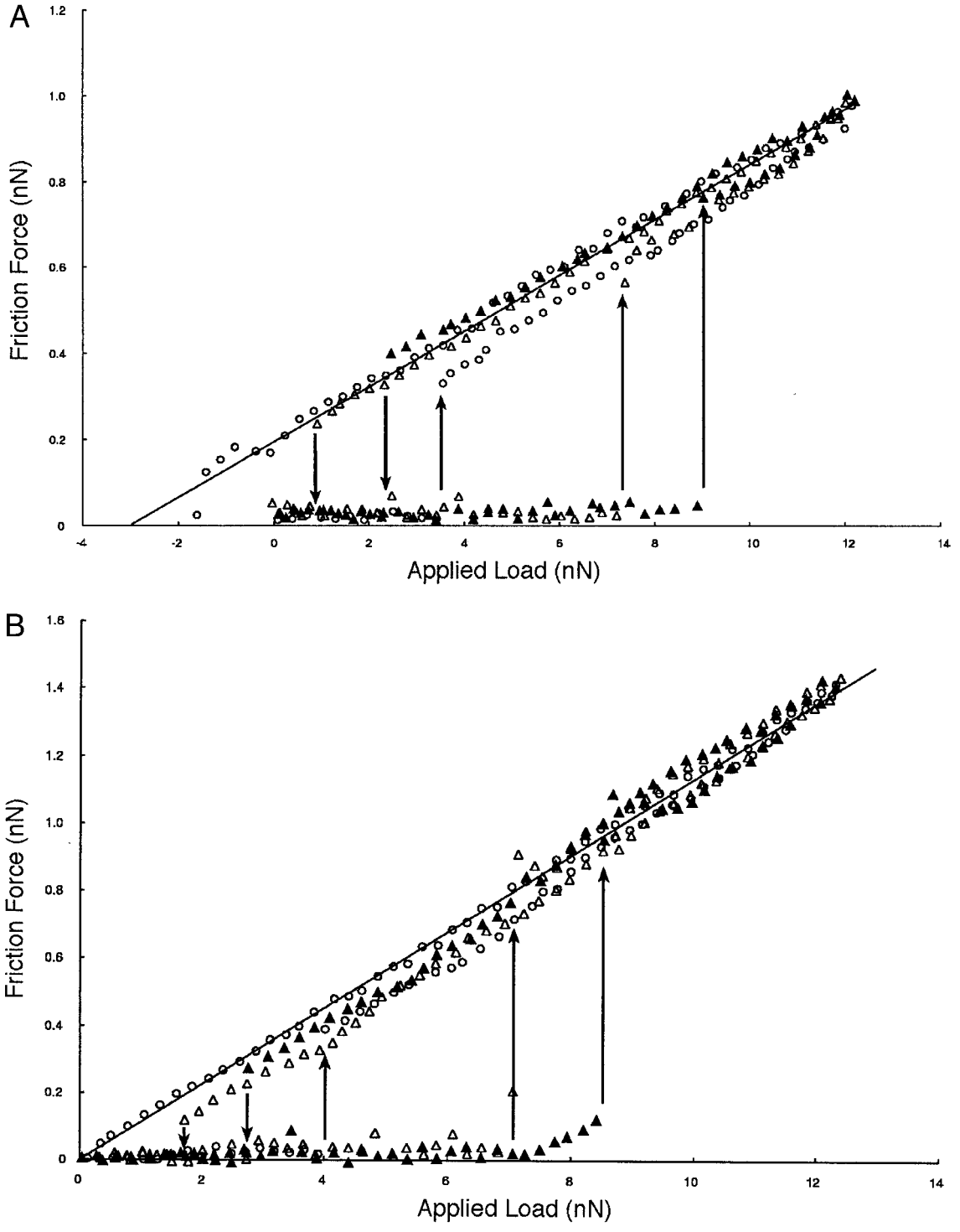

FIGURE 7 The lateral friction force experienced by the tip as a function of applied load for the mixed DOPC and DDM films at silica at stages (*A*) 1 (○), 3 (◇), and 5 (◆) and (*B*) stages 2 (○), 4 (◇), and 6 (◆). The friction force remains very close to zero until the mechanical instability of the adsorbed film is reached (compare with Fig. 3). The arrows indicate the applied load where a large change in friction occurs, an upwards pointing arrow for puncture of the layer and a downwards pointing arrow where the layer heals and friction returns to zero force. The solid line shows a best fit from friction data obtained in water. The zero in applied load was taken as the force where the feedback loop first began to track the surface as the force was increased; for this surface the feedback loop moved the piezo away from the surface at almost exactly the value as the force was decreased. Thus, there was no measurable adhesion for the lateral force mode.

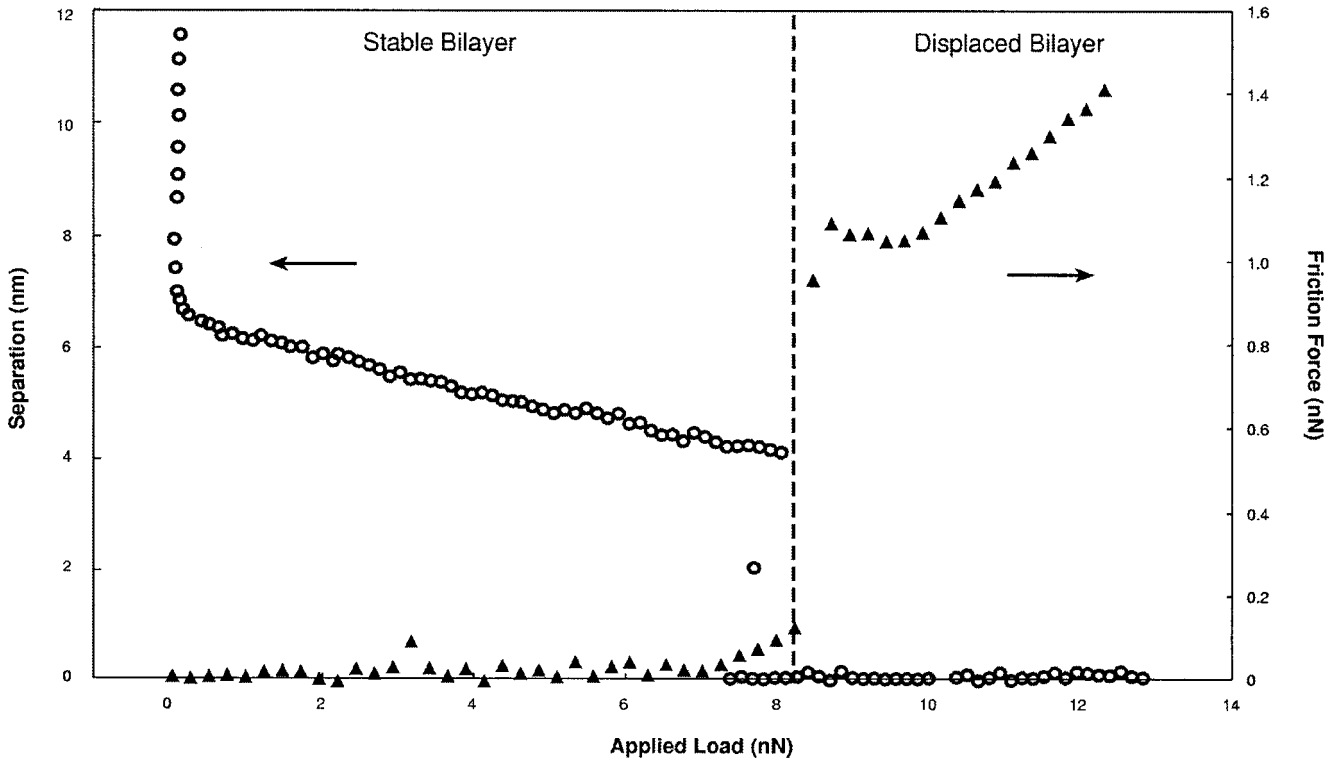

FIGURE 8 The separation (○) and friction force (▲) as a function of applied load for stage 6 on hydrophilic silica. This figure illustrates the strong correlation between the normal and lateral force data. As long as the supported bilayer is able to withstand the external pressure, the friction force remains very low; after the bilayer has been ruptured the friction force is approximately equal to that between the tip and surface in the absence of adsorbed material, i.e., pure water as the liquid phase. Note that only data for increasing applied load are shown.

the densely packed layer obtained at stage 6 (solid triangles), we note that the friction force is close to zero until the normal load has been increased above 7 nN. Then it starts to increase with the load and at about 8.5 nN a jump occurs to friction values similar to those between bare surfaces. This applied load value correlates well with critical breakthrough force for the normal force curve at the same DOPC surface coverage. Friction forces measured under decreasing loads are initially very similar to those measured between bare silica surfaces. Then a sudden drop of the friction force is observed when the applied load is reduced below a critical force, which in this case corresponds to the normal force at which surfaces in contact jump apart (cf. Fig. 3).

This behavior is different from that reported by Ducker and co-workers, who studied the friction force between surfaces with adsorbed short-chain lipids (Ducker and Clarke, 1994; Ducker et al., 1997). They also found that adsorbed lipid layers caused a shift of the friction force to lower values, but the measured friction coefficient not close to zero in the low load regime as observed in the present study. Our results suggest that the friction between the tip and the hydrated phosphatidylcholine headgroups is very low, corresponding to near perfect boundary lubrication and wear-less friction. If our observation is correct, there can be very little energy dissipated as the tip slides over the hydrated DOPC headgroups. Measurable friction values are indeed obtained only when the inner bilayer has ruptured or is strongly compressed.

Friction forces measured between surfaces in the asymmetric system with a lipid monolayer present on the underlying hydrophobized silica support

Friction-load curves were also measured for the asymmetric system where the silica tip slides on a hydrophobized silica surface. The data from this measurement are presented in Fig. 9, *A* and *B*. The main trends seen for the asymmetric system are the same as for the symmetric system. The force-load curve is linear with a slightly lower friction coefficient of ~0.07. Due to the adhesion between the tip and the solid surface, nonzero friction is also measured at negative applied loads. The finding of a lower friction coefficient between asymmetric compared with symmetric systems agree with earlier published results by Noy and co-workers (1995). The friction force is again very low until the breakthrough normal force is achieved. A significant increase in the friction force is, however, observed close to

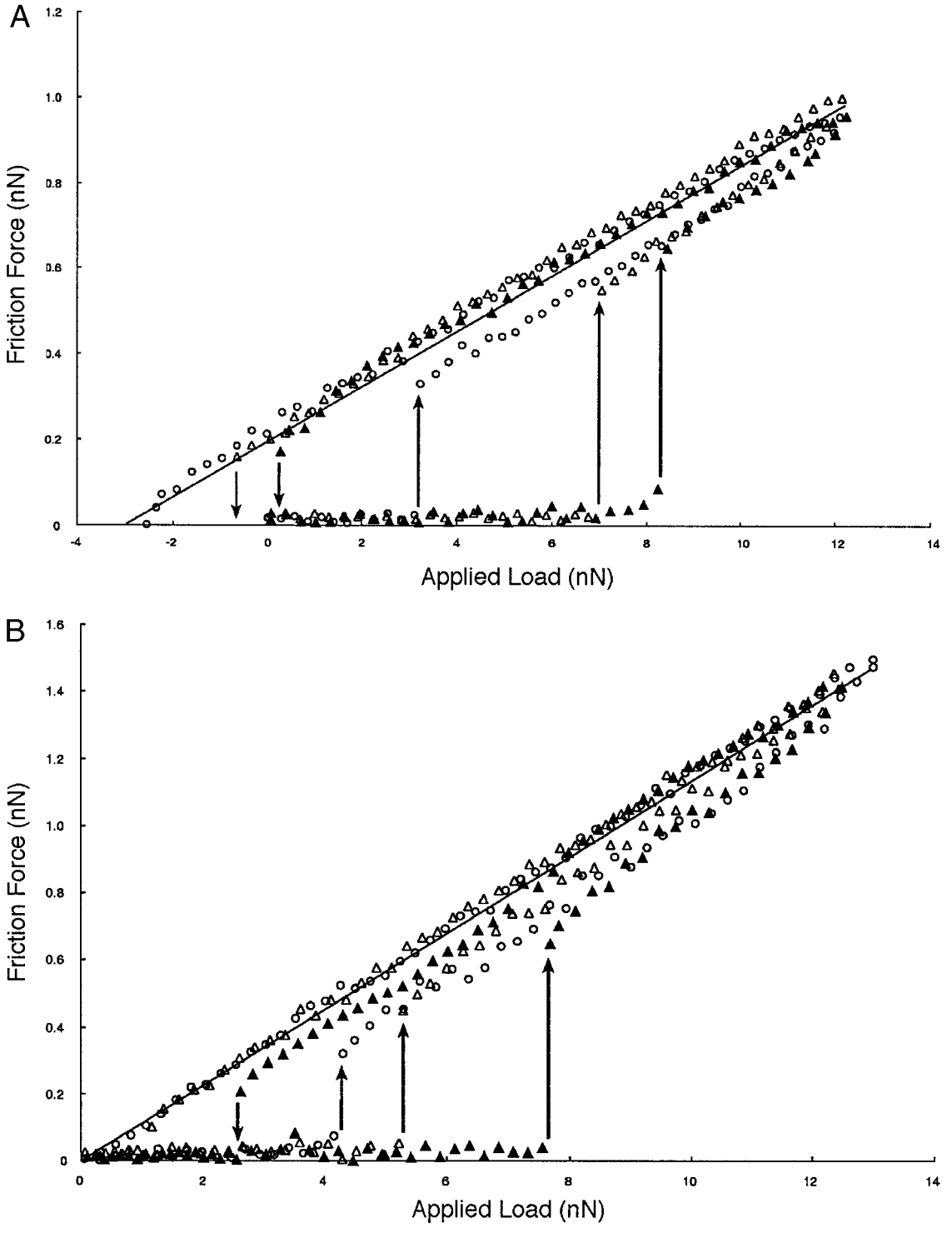

FIGURE 9 The lateral friction force experienced by the tip as a function of applied load for the mixed DOPC and DDM films of stages (*A*) 1 (○), 3 (◇), and 5 (◆) and (*B*) stages 2 (○), 4 (◇), and 6 (◆). Again the friction force remains very close to zero until the mechanical instability of the adsorbed film is reached (compare with Fig. 5). The arrows indicate the applied load where a large change in friction occurs, an upwards pointing arrow for puncture of the layer and a downwards pointing arrow where the layer heals and friction returns to approximately zero force. The solid line shows a best fit from friction data obtained in the water. The zero in applied load was taken as the force where the feedback loop first began to track the surface as the force was increased.

the critical load where the adsorbed layer can no longer support the tip. As the force exceeds the maximum supportable load an abrupt change in the friction force is observed and the friction force increases to values close to those measured in the absence of DOPC. As the load is reduced, a friction jump in the opposite direction is observed for the more densely packed layers. These sudden, hysteretic changes in friction force correlate well with the jump-in and jump-out values seen in the force curves in Fig. 5. The establishment of the fact that there is a clear correlation between the friction and normal force curves, which appears general for all layer structures and substrate systems studied, is an important contribution of the present work.

SUMMARY

Force-distance curves between surfaces with adsorbed DOPC bilayers show the following general characteristics. 1) There is an onset of a repulsive force when the hydrated phosphatidylcholine headgroups begin to interact. The slope of the barrier mirrors in a complex manner the contributions of both hydration/steric, mechanical interactions, effects that overlap and cannot easily be deconvoluted. 2) A jump into contact is observed when the tip starts penetrating the layer supported by the underlying flat substrate. 3) The jump-in distances measured on silica and hydrophobized silica correspond to the thickness of a slightly compressed bilayer and monolayer, respectively. 4) The barrier height is determined by the affinity to the solid and the lipid interchain cohesion but seems rather insensitive to the amount of co-adsorbed DDM. 5) The barrier heights were only slightly higher on hydrophobic compared with hydrophilic surfaces. 6) A hysteresis in the force curves measured on approach and separation is observed. This probably arises due to hydrodynamic effects associated with the penetration and healing of the adsorbed bilayer, respectively. 7) Surfaces pushed in contact are often spontaneously separated at positive applied loads by the surface pressure of the lipid layers surrounding the contacting surfaces.

The lateral force (friction) curves may be summarized as follows. 1) The friction forces measured between bare silica surfaces and between bare silica and hydrophobized silica show a linear dependence on the applied load, suggesting multiple asperity contacts between the sharp tip and the solid surface. 2) The applied load required to displace adsorbed material during lateral motion is very similar to that measured during a fixed position normal force measurement. 3) Adsorbed DOPC layers reduce the friction force markedly to values below the detection limit of the measurement technique as long as the inner DOPC layer is not punctured. 4) A large jump in the measured friction force is observed close to the critical breakthrough force values, which is followed by a linear friction versus load regime with only slightly lower friction values compared with those measured between bare surfaces. 5) The friction hysteresis loop observed when comparing inwards and outwards cycles relates to hysteresis in the critical jump-in and jump-out values seen in the normal force curves.

The very low friction measured between the AFM tip and the lipid-covered surface indicates that these molecules are well-suited boundary lubricants. Lipids have indeed been suggested to play an important biological role in joint surface lubrication (Hills 1989, 2000). Measurable friction forces were recorded only once the lipid layers were ruptured. The critical load for lipid layer rupture is estimated to be larger than 10 kg/cm^2 for all layers studied, which by physiological standards is considered to be relatively high. More accurate numbers cannot be given due to the uncertainty in contact area between the AFM tip and the underlying surface. The fact that no friction force could be detected between the tip and the intact lipid layers implies furthermore that friction contrast images on this type of system can only be obtained under conditions when lipid layers are strongly disrupted.

This work was sponsored by the Swedish Foundation for Strategic Research.

REFERENCES

Afshar-Rad, T., A. Bailey, P. Luckham, W. MacNaughtan, and D. Chapman. 1986. Direct measurement of forces between lipid bilayers. *Faraday Discuss. Chem. Soc.* 1–10:239–249.

Bayerl, T. M., and M. Bloom. 1990. Physical properties of single phospholipid bilayers adsorbed to micro glass beads: a new vesicular model system studied by ^{2}H-nuclear magnetic resonance. *Biophys. J.* 58:357.

Bergenståhl, B. A., and P. Stenius. 1987. Phase diagrams of dioleoylphosphatidylcholine with formamide, methyl formamide, and dimethylformamide. *J. Phys. Chem.* 91:5944–5948.

Bowden, F. P., and D. Tabor. 1967. Friction and Lubrication. John Wiley and Sons, New York.

Brinck, J., B. Jönsson, and F. Tiberg. 1998. Kinetics of nonionic surfactant adsorption and desorption at the silica-water interface: binary systems. *Langmuir.* 14:5863.

Capella, B., and G. Dietler. 1999. Force-distance curves by atomic force microscopy. *Surface Sci. Rep.* 34:1–104.

Derjaguin, B. 1934. Untersuchungen uber die reibung und adhesion, IV. *Kolloid Zeits.* 69:155–164.

Ducker, W. A., and D. R. Clarke. 1994. Controlled modification of silicon-nitride interactions in water via zwitterionic surfactant adsorption. *Colloids Surfaces A.* 93:275–292.

Ducker, W. A., and L. M. Grant. 1996. Effect of substrate hydrophobicity on surfactant-aggregate geometry. *J. Phys. Chem.* 100:11507–11511.

Ducker, W. A., E. P. Luther, D. R. Clarke, and F. E. Lange. 1997. Effect of zwitterionic surfactants on interparticle forces, rheology, and particle packing of silicon nitride slurries. *J. Am. Ceram. Soc.* 80:575–583.

Dufrene, Y. F., W. R. Barger, J. B. D. Green, and G. U. Lee. 1997. Nanometer-scale surface properties of mixed phospholipid monolayers and bilayers. *Langmuir.* 13:4779–4784.

Dufrene, Y. F., T. Boland, J. W. Schneider, W. R. Barger, and G. U. Lee. 1998. Characterization of the physical properties of model biomembranes at the nanometer scale with the atomic force microscope. *Faraday Discuss.* 79–94.

Dufrene, Y. F., and G. U. Lee. 2000. Advances in the characterization of supported lipid films with the atomic force microscope. *Biochim. Biophys. Acta Biomembr.* 1509:14–41.

Eskilsson, K., B. W. Ninham, F. Tiberg, and V. V. Yaminsky. 1998. Interaction between hydrophilic surfaces in triblock copolymer solution. *Langmuir.* 14:7287–7291.

Giesen, P. L. A., G. M. Willems, H. C. Hemker, and W. T. Hermens. 1991. Membrane mediated assembly of the prothrombinase complex. *Biol. Chem.* 266:18720.

Grant, L. M., and W. A. Ducker. 1997. Effect of substrate hydrophobicity on surface-aggregate geometry: Zwitterionic and nonionic surfactants. *J. Phys. Chem. B.* 101:5337–5345.

Grant, L. M., T. Ederth, and F. Tiberg. 2000. Influence of surface hydrophobicity on the layer properties of adsorbed nonionic surfactants. *Langmuir.* 16:2285–2291.

Hills, B. A. 1989. Oligolamellar lubrication of joints by surface active phospolipid. *J. Rheumatol.* 16:82–91.

Hills, B. A. 1995. Remarkable antiwear properties of joint surfactant. *Ann. Biomed. Eng.* 23:112–115.

Hills, B. A. 2000. Boundary lubrication in vivo. *Proc. Inst. Mech. Eng. H J. Eng. Med.* 214:83–94.

Hines, J. D., R. K. Thomas, P. R. Garrett, G. K. Rennie, and J. Penfold. 1998. A study of the interactions in a ternary surfactant system in micelles and adsorbed layers. *J. Phys. Chem. B.* 102:9708.

Israelachvili, J. N. 1994. Strength of van der Waals attraction between lipid bilayers. *Langmuir.* 10:3369–3370.

Johnson, T., T. M. Bayerl, D. C. McDermott, G. W. Adam, A. R. Rennie, R. K. Thomas, and E. Sackmann. 1991. Structure of an adsorbed dimyristoylphosphatidylcholine bilayer measured with specular reflection of neutrons. *Biophys. J.* 59:289.

Johnston, S. A. 1997. Osteoarthritis: joint anatomy, physiology, and pathobiology. *Vet. Clin. North Am. Small Animal Prac.* 27:699.

Kop, J. M. M., P. A. Cuypers, T. Lindout, H. C. Hemker, and W. T. Hermens. 1984. The adsorption of prothrombin to phospholipid monolayers quantified by ellipsometry. *J. Biol. Chem.* 259:13933.

Larsson, K. 1994. Lipids: Molecular Organisation, Physical Functions, and Technical Applications. The Oily Press, Dundee, UK.

Lis, L. J., M. McAlister, N. Fuller, R. P. Rand, and V. A. Parsegian. 1982. Measurements of the lateral compressibility of several phospholipid bilayers. *Biophys. J.* 37:667.

Malmsten, M. 1995. Protein adsorption at phospholipid surfaces. *J. Colloid Interface Sci.* 17:106.

Manne, S., and H. E. Gaub. 1997. Force microscopy: measurement of local interfacial forces and surface stresses. *Curr. Opin. Colloid Interface Sci.* 2:145–152.

Marra, J. 1985. Controlled deposition of lipid monolayers and bilayers onto mica and direct force measurements between galactolipid bilayers in aqueous solutions. *J. Colloid Interface Sci.* 107:446–458.

Marra, J., and J. Israelachvili. 1985. Direct measurements of forces between phosphatidylcholine and phosphatidylethanolamine bilayers in aqueous electrolyte solutions. *Biochemistry.* 24:4608–4618.

McConnell, H. M., T. H. Watts, R. M. Weis, and A. A. Brian. 1986. Supported planar membranes in studies of cell-cell recognition in the immune system. *Biochim. Biophys. Acta.* 864:95–106.

Noy, A., D. Frisbie, L. F. Rozsnyai, M. S. Wrighton, and C. M. Lieber. 1995. Chemical force microscopy: exploiting chemically-modified tips to quantify adhesion, friction, and functional group distribution in molecular assemblies. *J. Am. Chem. Soc.* 117:7943–7951.

Sackman, E. 1996. Supported membranes: scientific and practical applications. *Science.* 271:43–48.

Schneider, J., Y. F. Dufrene, W. R. Barger, and G. U. Lee. 2000. Atomic force microscope image contrast mechanisms on supported lipid bilayers. *Biophys. J.* 79:1107–1118.

Schwarz, I. M., and B. A. Hills. 1998. Surface-active phospholipid as the lubricating component of lubricin. *Br. J. Rheumatol.* 37:21–26.

Senden, T. J. 2001. Force microscopy and surface interactions. *Curr. Opin. Colloid Interface Sci.* 6:95–101.

Solletti, J. M., M. Botreau, F. Sommer, W. L. Brunat, S. Kasas, T. M. Duc, and M. R. Celio. 1996. Elaboration and characterization of phospholipid Langmuir- Blodgett films. *Langmuir.* 12:5379–5386.

Tiberg, F. 1996. Physical characterization of nonionic surfactant layers adsorbed at hydrophilic and hydrophobic surfaces by time-resolveed ellipsometry. *J. Chem. Soc. Faraday Trans.* 92:531.

Tiberg, F., J. Brinck, and L. Grant. 1999. Adsorption and surface-induced self-assembly of surfactants at the solid-aqueous interface. *Curr. Opin. Colloid Interface Sci.* 4:411–419.

Tiberg, F., and T. Ederth. 2000. Interfacial properties of nonionic surfactants and decane-surfactant microemulsions at the silica-water interface: an ellipsometry and surface force study. *J. Phys. Chem. B.* 104: 9689–9695.

Tiberg, F., I. Harwigsson, and M. Malmsten. 2000. Formation of model lipid bilayers at the silica-water interface by co-adsorption with nonionic dodecyl maltoside surfactant. *Eur. Biophys. J.* 29:196–203.

Tiberg, F., B. Jönsson, and B. Lindman. 1994. Ellipsometry studies of the self-assembly of nonionic surfactants at the silica-water interface: kinetic aspects. *Langmuir.* 10:3714.

Voet, D., and J. G. Voet. 1990. Biochemistry. John Wiley and Sons, New York.

Warr, G. G. 2000. Surfactant adsorbed layer structure at solid/solution interfaces: impact and implications of AFM imaging studies. *Curr. Opin. Colloid Interface Sci.* 5:88–94.